

DYNAMICAL MASSES OF LOW MASS STARS IN THE TAURUS AND OPHIUCHUS STAR FORMING REGIONS

M. SIMON^{1,8}, S. GUILLOTEAU², E. DI FOLCO², A. DUTREY², N. GROSSO³, V. PIÉTU⁴, E. CHAPILLON^{2,4}, L. PRATO⁵, G.H. SCHAEFER⁶, E. RICE^{7,8}, Y. BOEHLER⁹

¹Dept. of Physics and Astronomy, Stony Brook University, Stony Brook, NY 11794-3800, USA; michal.simon@stonybrook.edu

²Laboratoire d'astrophysique de Bordeaux, Univ. Bordeaux, CNRS, B18N, alle Geoffroy Saint-Hilaire, 33615 Pessac, France

³Université de Strasbourg, CNRS, Observatoire Astronomique de Strasbourg, UMR 7550, 67000 Strasbourg, France

⁴IRAM, 300 rue de la piscine, F-38406 Saint Martin d'Hères, France

⁵Lowell Observatory, 1400 West Mars Hill Road, Flagstaff, AZ 86001, USA

⁶The CHARA Array of Georgia State University, Mount Wilson Observatory, Mount Wilson, CA 91023, USA

⁷Dept. of Engineering Science and Physics, College of Staten Island, Staten Island, NY 10314, USA

⁸Dept. of Astrophysics, American Museum of Natural History, New York, NY 10024, USA

⁹Physics and Astronomy Dept., Rice University, Houston, TX 77005-1827, USA

ABSTRACT

We report new dynamical masses for 5 pre-main sequence (PMS) stars in the L1495 region of the Taurus star-forming region (SFR) and 6 in the L1688 region of the Ophiuchus SFR. Since these regions have VLBA parallaxes these are absolute measurements of the stars' masses and are independent of their effective temperatures and luminosities. Seven of the stars have masses $< 0.6 M_{\odot}$ thus providing data in a mass range with little data, and of these, 6 are measured to precision $< 5\%$. We find 8 stars with masses in the range 0.09 to $1.1 M_{\odot}$ that agree well with the current generation of PMS evolutionary models. The ages of the stars we measured in the Taurus SFR are in the range 1-3 MY, and < 1 MY for those in L1688. We also measured the dynamical masses of 14 stars in the ALMA archival data for Akeson & Jensen's Cycle 0 project on binaries in the Taurus SFR. We find that the masses of 7 of the targets are so large that they cannot be reconciled with reported values of their luminosity and effective temperature. We suggest that these targets are themselves binaries or triples.

Keywords: stars: pre-main sequence, masses – techniques: mm-wave interferometry

1. INTRODUCTION

Astronomers deduce the masses and ages of stars by their positions on Hertzsprung-Russell diagrams (HRDs) relative to models of stellar evolution and their isochrones. This procedure is regarded as reliable for stars on the main sequence or approaching it. The reasons for this confidence are that the theoretical models for these stars are in good agreement, that the models are calibrated by many accurate and precise measurements of stellar masses, and that the properties of the stars are well-understood. The situation is more problematic for pre-main sequence (PMS) stars. For stars of young age, age $< \sim 10$ MY, and low mass, $< \sim 1 M_{\odot}$, there has been considerable scatter among the models of their evolution, precise measurements of their masses are sparse, and measurements of properties such as the luminosity and effective temperature are often complicated by activity associated with PMS stars. Among the reasons why this gap in our understanding needs to be filled is that we now know that it includes the era of planet formation among sun-like stars.

In this paper we present new dynamical masses of single, low mass young stars measured by the rotation of their circumstellar disks e.g. [Guilloteau et al. \(2014\)](#). We focused our ALMA Cycle 2 program on young stars expected to have masses smaller than $0.5 M_{\odot}$ on the basis of their spectral types. The measured masses are absolute because our targets are at known distances. We measured 5 new masses in the L1495 region of Taurus and 6 in the L1688 region of Ophiuchus, all with high precision.

We also used archival data from [Akeson & Jensen \(2014\)](#)'s ALMA program designed to study the disks of the components of young binaries in the Taurus SFR. We were able to measure 14 new dynamical masses, most more massive than the stars in our ALMA program. Seven of these new measurements probably represent the detection of

new multiples that are angularly unresolved at present.

For simplicity we designate the two data sets we use in this paper as follows. ALMA Cycle 2 refers to data obtained for our project on single stars in Taurus (L1495) and Ophiuchus (L1688) (ALMA Project 2013.2.00163.S). ALMA Cycle 0 designates [Akeson & Jensen \(2014\)](#)'s project (AJ14) directed at binaries distributed over the Taurus SFR (ALMA Project 2011.0.00150.S).

2. TARGETS

2.1. ALMA Cycle 2: Taurus and Ophiuchus

We sought to observe single stars with circumstellar disks expected on the basis of their spectral types to have masses $< \sim 0.5 M_{\odot}$ and to lie at known distances. We proceeded as follows:

1) *Star Forming Regions (SFRs)*: We chose to observe PMS stars in the Taurus and Ophiuchus SFRs because lying at average distances 140 and 120 pc, respectively, they are relatively nearby ([Kenyon et al. 2008](#); [Wilking et al. 2008](#)).

Also, extensive recent studies of their members are available: [Andrews et al. \(2013, And13\)](#) and [Herczeg & Hillenbrand \(2014, He14\)](#) for Taurus; [Ricci et al. \(2010a, R10a\)](#), [McClure et al. \(2010\)](#), and [Najita et al. \(2015\)](#) for Ophiuchus.

2) *Distances, Environments, and Ages*: PMS stars in the Taurus and Ophiuchus SFRs are mostly located in small dark clouds ([Lynds 1962](#)) which are also identifiable in CO ([Dame et al. 2001](#), see for example Fig. 6 in [Guilloteau et al. 2014](#)). Several of these stellar groups have measured distances more precise than the averages to the Taurus and Ophiuchus SFRs. Three stars in L1495 in Taurus have VLBA parallaxes placing its average distance at 131.4 ± 2.4 pc ([Torres et al. 2012](#)). Two stars in L1688 in Ophiuchus have VLBA parallaxes ([Loiuard et al. 2008](#)). We use their average, 119.4 ± 4.6 pc for the distance to L1688. We drew our targets from the L1495 and L1688 regions. The environments of these regions are quite different. The stellar and molecular gas density in L1688 in Ophiuchus is far greater ([Wilking et al. 2008](#)) than in the L1495 in Taurus ([Kenyon et al. 2008](#)). We were interested to learn whether observations of the two regions would provide information on environmental effects on the measurement of stellar masses by disk rotation.

Table 1 lists the stars observed in the Taurus L1495 region. All are Class II YSOs. Columns 1 and 2 provide an ID and name. Cols. 3, 4, and 5 list the spectral type, effective temperature, and luminosity as listed by And13 and cols. 6, 7, and 8 provide the same parameters as provided by He14. We did not propagate the distance uncertainty into the uncertainty of the luminosity. And13's spectral types are drawn from the literature. We used their listing of the corresponding T_{effs} and uncertainties. He14 derived stellar parameters from an analysis of a large homogeneous set of spectra in the visible. Col. 6 lists He14's independent SpTy assignments and col. 7 gives the corresponding T_{effs} using their conversion table and their recommended uncertainty of ± 0.3 sub-type. We highlighted in bold the cases for which the And13 and He14 spectral type designations differ by more than one subclass. Taking together this sample and Akeson and Jensen's (see §2.2) there is no clear pattern that one set of spectral types is hotter or cooler than the other in the spectral type range considered. And13 derived luminosities and their uncertainties from spectral energy distributions (SEDs). Since And13's values are calculated at the 140 pc average distance to the Taurus SFR we scaled them to the 131 pc distance of L1495. He14 derived luminosities using their observed spectra referred to the BT/Settl models at $\log g = 4.0$ provided by [Allard et al. \(2012\)](#). We list He14's luminosities with their recommended uncertainty ± 0.2 dex. He14 evaluated these luminosities at 131 pc. The last star in the table, FM Tau, was not a part of our ALMA program; it was observed in CO J=2-1 by Y. Boehler et al. in ALMA project 2013.2.00426.S using the same antenna configuration as our Taurus observations on Jul. 19 and Aug 8, 2015, and in CO J=3-2 on Jul 24, 2015 with about $0.3''$ resolution. CX Tau was also observed in this project.

Table 1 also provides the same parameters for selected stars in the Ophiuchus SFR. All are in L1688. Except for the Flying Saucer (2MASS J16281370-2431391 [Grosso et al. 2003](#)), the stellar parameters are from [Ricci et al. \(2010a, R10a\)](#) and [Najita et al. \(2015\)](#). We converted the SpTy's to T_{effs} using the look-up table from [Pecaut & Mamajek \(2013\)](#), applied an uncertainty of ± 1 sub-type. R10a evaluated the luminosities from the stars' near IR SEDs after dereddening the near IR colors and correcting for extinction. Their values are given for a distance of 130 pc; accordingly we scaled the luminosities to the 119 pc distance adopted here for the L1688 region and applied an uncertainty of ± 0.13 dex as suggested in [Ricci et al. \(2010b\)](#). Luminosities listed by [Najita et al. \(2015\)](#) are based on the analysis of [McClure et al. \(2010\)](#) of Spitzer Observatory observations. The luminosities are presented at the distance of L1688 and do not include a propagated distance uncertainty. The uncertainties depend on extinction to the star; we used values kindly provided by McClure (priv. comm.). We converted the spectral types to T_{effs} using Pecaut and Mamajek's look-up table again. [McClure et al. \(2010\)](#) identify all the stars as Class II PMS stars except for GSS 26 and GY 284 listed as flat spectrum sources (FS) and YLW16C (= GY 262) for which a designation is not available

Table 1. Stellar Properties in Taurus L1495 and Ophiuchus L1688

ID	Name	SpTy	$\log T_{\text{eff}}$	$\log L/L_{\odot}$	SpTy	$\log T_{\text{eff}}$	$\log L/L_{\odot}$
			Andrews et al. (2013)			Herczeg & Hillenbrand (2014)	
Stars in L1495							
Bold identifies spectral types differing by more than one subclass (see text)							
1	FN Tau	M5	3.495 ± 0.020	-0.140 ± 0.097	M3.5	3.516 ± 0.013	-0.20 ± 0.20
2	MHO 1	M2.5	3.543 ± 0.018	0.172 ± 0.883	N/A		
3	CIDA 1	M5.5	3.485 ± 0.020	-0.959 ± 0.089	M3.5	3.516 ± 0.013	-0.72 ± 0.20
4	CY Tau	M1.5	3.560 ± 0.017	-0.456 ± 0.090	M2.5	3.542 ± 0.006	-0.58 ± 0.20
5	FP Tau	M4	3.514 ± 0.019	-0.549 ± 0.048	M2.6	3.540 ± 0.006	-0.78 ± 0.20
6	CX Tau	M2.5	3.543 ± 0.015	-0.489 ± 0.065	M2.5	3.542 ± 0.006	-0.58 ± 0.20
7	V410 X-Ray 1	M4	3.514 ± 0.019	-0.409 ± 0.066	M3.7	3.507 ± 0.013	-1.55 ± 0.20
8	IP Tau	M0	3.586 ± 0.024	-0.389 ± 0.126	M0.6	3.583 ± 0.006	-0.47 ± 0.20
9	FM Tau	M0	3.586 ± 0.024	-0.45 ± 0.12	M4.5	3.489 ± 0.012	-1.15 ± 0.20
ID	Name	SpTy	$\log T_{\text{eff}}$	$\log L/L_{\odot}$	SpTy	$\log T_{\text{eff}}$	$\log L/L_{\odot}$
			Ricci et al. (2010b)			Najita et al. (2015), McClure et al. (2010)	
Stars in L1688							
1	GSS 26	K8	3.599 ± 0.010	0.14 ± 0.13	K7	3.609 ± 0.023	0.91 ± 0.60
2	GSS 39	M0	3.586 ± 0.021	-0.11 ± 0.13	M0	3.586 ± 0.024	0.11 ± 0.24
3	YLW16C	M1	3.566 ± 0.020	0.045 ± 0.13	M1	3.569 ± 0.017	0.14 ± 0.25
4	ROXs 25	M2	3.550 ± 0.018	0.45 ± 0.13	K7	3.609 ± 0.023	0.49 ± 0.09
5	YLW 58	M4	3.505 ± 0.020	-0.64 ± 0.13	M4.5	3.495 ± 0.019	-0.70 ± 0.04
6	Flying Saucer		3.544 ± 0.040	-1.05 ± 0.13	See text for Flying Saucer Parameters		
7	WL 18	N/A			K6.5	3.615 ± 0.016	-0.57 ± 0.13
8	WL 14	N/A			M4	3.514 ± 0.019	-0.85 ± 0.15
9	GY 284	N/A			M3.25	3.525 ± 0.018	-0.92 ± 0.05

from the SED slope between 2 and 25 μm (but for which an envelope is excluded from the SED slope between 5 and 12 μm). The Flying Saucer is an edge-on disk dominated by scattered light; its parameters are from [Grosso et al. \(2003\)](#) and [Pontoppidan et al. \(2007\)](#). Both groups assumed a [Kurucz \(1979\)](#) stellar atmosphere model at $T_{\text{eff}} = 3500\text{K}$ to derive the luminosity of the central star from SED modeling. From an extinction map around the Flying Saucer, [Grosso et al. \(2003\)](#) derived $A_v = 2.1$ mag and $L_*/L_{\odot} = 0.14$ at a distance of 140 pc corresponding to $L_*/L_{\odot} = 0.10$ at 119 pc. [Pontoppidan et al. \(2007\)](#) assumed $A_v = 0.50$ mag, added an accretion luminosity $L_{\text{acc}}/L_{\odot} = 0.6$ and $L_*/L_{\odot} = 0.084$ at 125 pc which scales to $L_*/L_{\odot} = 0.076$ at 119 pc. In Table 1 we quote the T_{eff} with an uncertainty of $\pm 200\text{K}$ which corresponds to approximately to one spectral class sub-type at $\sim 3500\text{K}$, and the luminosity as an average of the two values 0.089 ± 0.025 with the uncertainty equal to the range. The derived stellar luminosity depends on the assumed foreground extinction. The uncertainty of the Flying Saucer’s luminosity may be larger than the value we adopt.

2.2. ALMA Cycle 0: Taurus

AJ14 obtained ALMA Cycle 0 observations of 17 young binaries in the Taurus SFR. We list their targets in Table 2 in the same format as Table 1. The components of the binaries in their program are mostly of earlier spectral type than in ours. GK Tau, HO Tau, and DS Tau, are probably single because AJ14 found that their presumed companions seem to be chance associations. Most of the stars in their sample are distributed over the Taurus SFR; we consider 140 pc as their distance. However, we can assign a more precise value for 2 stars, GK Tau and HO Tau. GK Tau’s position ($l=174.2$, $b=-15.7$) places it near L1495: we assume its distance is 131 pc. HO Tau lies near the star HP Tau/G2 which has a VLBA parallax measurement $161.2 \pm 0.09\text{pc}$ ([Torres et al. 2009](#)). These stars seem to be associated with L1529 region. We assume both lie at 161 pc.

3. OBSERVATIONS, DATA REDUCTION, AND ANALYSIS

3.1. Observations

Table 2. Stellar Properties Akeson&Jensen Archival Data

ID	Name	SpTy	log T_{eff}	log L/L_{\odot}	SpTy	log T_{eff}	log L/L_{\odot}
			Andrews et al. (2013)		Herczeg & Hillenbrand (2014)		
		Bold identifies spectral types differing by more than one subclass (see text)					
1	FV Tau A	K5	3.639 ± 0.024	0.369 ± 0.143	M0.0	3.591 ± 0.006	-0.48 ± 0.20
2	FX Tau A	M1	3.569 ± 0.017	-0.285 ± 0.215	M2.2	3.545 ± 0.008	-0.29 ± 0.20
3	HBC 411 B	M4.5	3.505 ± 0.039	-0.699 ± 0.130	M4.3	3.501 ± 0.004	-0.80 ± 0.20
4	CIDA-9 A	K8	3.601 ± 0.023	-1.010 ± 0.255	M1.8	3.560 ± 0.005	-0.88 ± 0.20
5A	HK Tau A	M0.5	3.577 ± 0.020	-0.353 ± 0.126	M1.5	3.564 ± 0.007	-0.52 ± 0.20
5B	HK Tau B	M2	3.552 ± 0.020	-1.571 ± 0.194	N/A		
6	IT Tau B	M4	3.515 ± 0.019	-0.684 ± 0.165	K6.0	3.615 ± 0.003	-0.01 ± 0.20
7A	DK Tau A	K8	3.601 ± 0.023	0.119 ± 0.189	K8.5	3.599 ± 0.003	-0.27 ± 0.20
7B	DK Tau B	M1	3.569 ± 0.020	-0.498 ± 0.158	M1.7	3.560 ± 0.006	-0.76 ± 0.20
8	GK Tau	K7	3.609 ± 0.023	0.129 ± 0.234	K6.5	3.609 ± 0.003	-0.03 ± 0.20
9	HN Tau A	K5	3.639 ± 0.024	-0.376 ± 0.365	K3	3.657 ± 0.006	-0.77 ± 0.20
10	V710 Tau A	M0.5	3.577 ± 0.020	-0.241 ± 0.124	M3.3	3.524 ± 0.009	-0.43 ± 0.20
11	HO Tau	M0.5	3.577 ± 0.020	-0.886 ± 0.087	M3.2	3.527 ± 0.008	-0.85 ± 0.20
12	DS Tau	K5	3.639 ± 0.024	-0.119 ± 0.162	M0.4	3.581 ± 0.007	-0.72 ± 0.20

ALMA 2013.2.00163.S— Our ALMA observations were made with a frequency setup covering the CO J=2-1 and H₂CO 3₁₃-2₁₂ transitions, as well as all the stronger hyperfine components of the CN N=2-1 line. The Ophiuchus targets were observed on May 23, 2015 with a baseline configuration that provided a typical angular resolution of $0.6'' \times 0.4''$ at PA 90°. The typical noise is ~ 7 mJy/beam (about 0.6 K in brightness) at 0.2 km s^{-1} spectral resolution. The Taurus targets were observed on Sept. 19, 2015 with the same frequency setup but a baseline configuration that provided a higher angular resolution $0.25'' \times 0.21''$ at PA 180° and hence a much higher brightness noise, typically about 3 K. We calibrated the data using the ALMA pipeline in the CASA software package (Version 4.2.2) and applied doppler correction using the “cvel” task to transform the data in the LSRK frame. Data were then exported through UVFITS format to the GILDAS package for imaging and data analysis. For all sources except WL 14 and GY 284 (which have no or weak signal), phase-only self-calibration solutions were derived from the continuum and applied to the spectral line tables. All data were smoothed to 0.2 km s^{-1} spectral resolution.

ALMA 2011.0.00150.S— AJ14’s spectral line observations were made in the CO J=2-1 and 3-2 lines. We processed data for both lines as above using CASA 3.4 software and exported it to GILDAS for imaging and analysis. The angular resolution of the J=2-1 data is about $0.85 \times 0.50''$ and the spectral resolution is 0.85 km s^{-1} . The typical brightness sensitivity is 0.5 K. The J=2-1 data has both lower angular resolution $1.0 \times 0.8''$ and spectral resolution 1.26 km s^{-1} , but the brightness sensitivity is around 0.15 K. In both cases, phase-only self-calibration was derived from the continuum data and applied to the spectral line data.

ALMA 2013.2.00426.S— In addition to our survey data, two sources observed in ALMA 2013.2.00426.S (PI Y.Boehler) in CO J=2-1 and CO J=3-2 were suitable for our purpose: CX Tau and FM Tau. The CO J=2-1 observations were done with similar velocity and angular resolutions and sensitivity as in 2012.2.00163.S, while the CO J=3-2 data provided about $0.3 \times 0.17''$ resolution, with about 3 K brightness sensitivity at 0.21 km s^{-1} spectral resolution.

Continuum images for the observed stars are shown in Fig.1-2. We do not report values of the continuum flux for two reasons. Quoting reliable uncertainties would imply a proper flux scale calibration which is not reliable in our data set. The absolute flux has no impact on our analysis which relies only on the morphology of the emission.

3.2. Analysis

We analyzed the data for disk parameters using the *DiskFit* tool (Piétu et al. 2007) exactly as in our earlier work (Guilloteau et al. 2014) and give details in Appendix A. Table 3 presents the results of ALMA Cycle 2 observations of the stars in Taurus and Ophiuchus. In our L1495 sample, ALMA did not detect a signal at V410 X-Ray 1, confusion at MHO 1-2, and confusion and weak signal at CIDA 1 prevented reliable measurements. We discuss the confusion

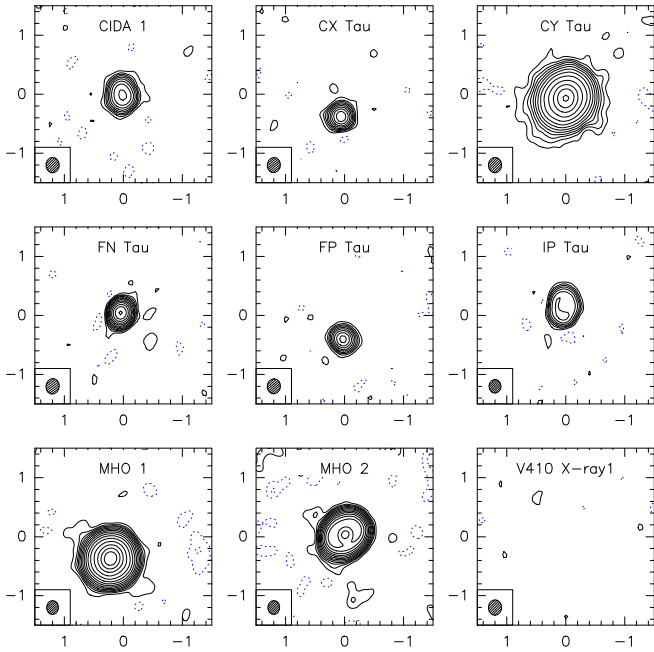


Figure 1. Continuum images at 228 GHz of the Taurus sources. Contour levels are -3,-2,-1,1,2,3 times the contour step (0.25 mJy/beam), and then increase exponentially by a factor $\sqrt{2}$.

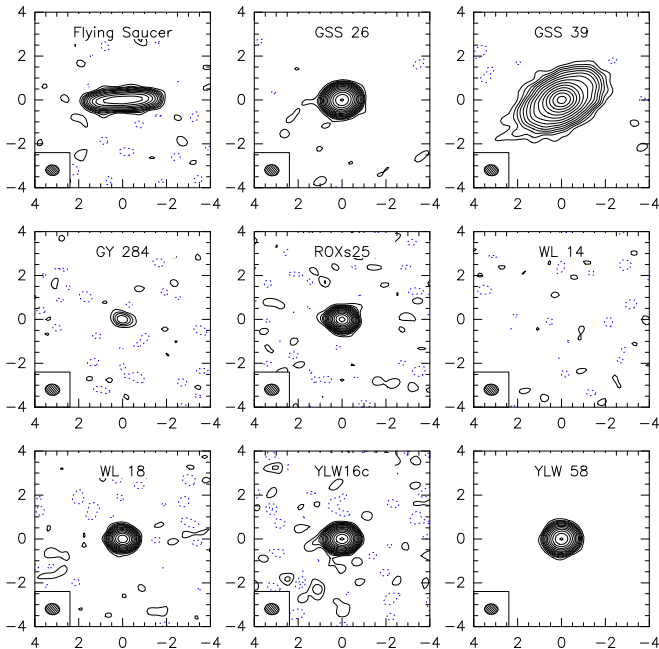


Figure 2. As Fig. 1 for ρ Oph sources. Contour step is 0.45 mJy/beam for GSS 26, GSS 39 and YLW 58, 0.15 mJy/beam for the other sources (approximately 2σ).

problem further in §5.4. No line emission was detected at FN Tau despite its strong continuum so we were unable to measure its mass. In L1688 we were unable to measure masses of WL 18, WL 14, and GY 284 because the line emission of their disks proved too weak for detection with the observational set-up we used. Spectral line images of the detected disks are given in Figs. 3 and B4-B8.

In Table 3 Columns 1 and 2 give the sample number and name. We assumed that the entire sample is associated with L1495 at its distance of 131 pc (Col. 3). We did not propagate uncertainties in the distance. Col. 4 lists the lines analyzed. Col. 5 gives the velocity of the line center with respect to the local standard of rest. Cols. 6 and 7 give the disk inclination as measured for the line, i_{line} , and continuum emission, i_{cont} ($i = 0$ corresponds to

Table 3. Measured Parameters in Taurus L1495 and Ophiuchus L1688

ID	Name	Dist pc	Lines	V_{LSR} km s^{-1}	i_{line} deg	i_{cont} deg	R_{out} AU	M_* M_{\odot}
Stars in L1495								
4	CY Tau	131	CO, CN	7.27 ± 0.03	30 ± 2	32 ± 1	290 ± 10	0.31 ± 0.02
5	FP Tau	131	CO, CN	8.32 ± 0.06	66 ± 2	66 ± 4	95 ± 5	0.37 ± 0.02
6	CX Tau	131	CO, CN	8.40 ± 0.03	61 ± 1	60 ± 5	160 ± 20	0.37 ± 0.02
8	IP Tau	131	CO, CN	6.30 ± 0.02	34 ± 1	35 ± 2	95 ± 20	0.95 ± 0.05
9	FM Tau	131	CO	5.98 ± 0.08	52 ± 2	55 ± 2	50 ± 2	0.36 ± 0.01
Stars in L1688								
1	GSS 26	119	CO	2.75 ± 0.01	40 ± 1	39 ± 1	325 ± 5	1.51 ± 0.02
2	GSS 39	119	CO, H ₂ CO	2.00 ± 0.01	54.3 ± 0.2	57 ± 2	600 ± 1	0.47 ± 0.01
3	YLW16C	119	H ₂ CO	5.43 ± 0.17	17 ± 1	17 ± 4	32 ± 2	1.80 ± 0.10
4	ROXs 25	119	CO, CN	4.94 ± 0.05	39 ± 4	44 ± 4	60 ± 3	1.10 ± 0.07
5	YLW 58	119	H ₂ CO	3.76 ± 0.04	30 ± 5	30 ± 1	130 ± 3	0.09 ± 0.01
6	Flying Saucer	120	CS	3.555 ± 0.003	85.4 ± 0.5	89.2 ± 0.4	200 ± 7	0.58 ± 0.01

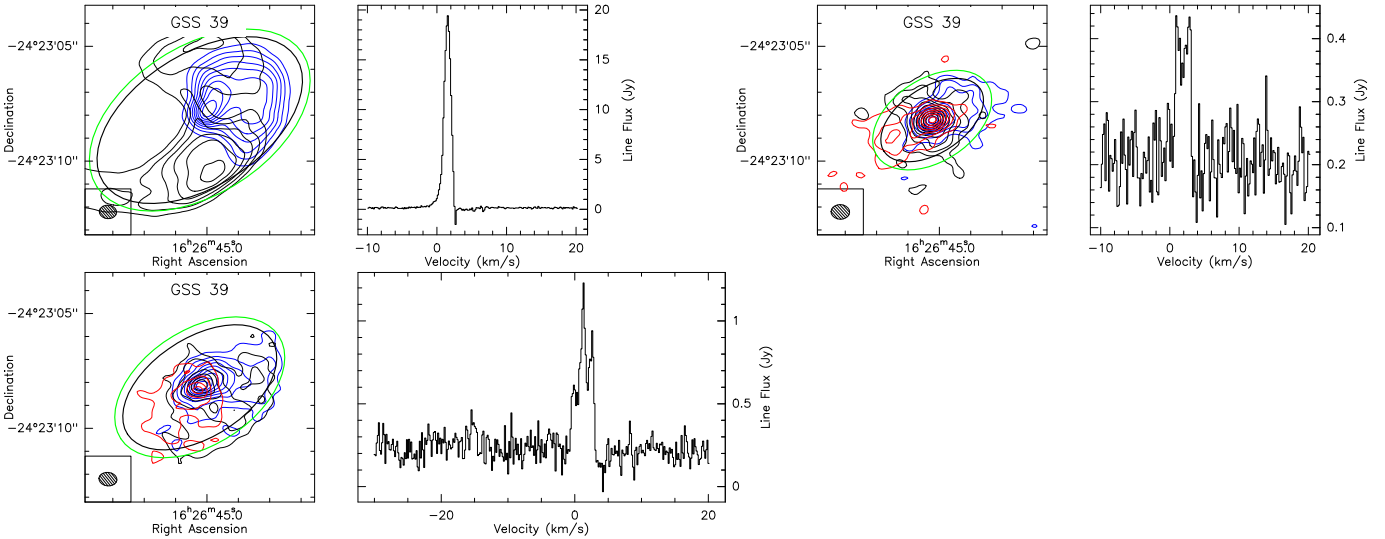


Figure 3. Molecules towards GSS 39: CO (top left), H₂CO (top right), CN (bottom). In the maps, red (resp. blue) contours indicate red-shifted (blue-shifted) emission, black contours emission near the systemic velocity. The black ellipse is the location of the disk outer radius, and the green ellipse the region used to derive the integrated spectra. The CN lines have hyperfine structure. See Appendix for other sources. .

face-on). Because the continuum emission arises from dust in the disk, its emission region is more compact than that of the line emission. Hence we were not able to measure i_{cont} reliably for all disks. Because an interferometer provides spatial measurements on an angular scale, radial distances in the disk scale as distance D to the star and because the disk is seen at an inclination along the line-of-sight, the velocity measured is the radial velocity. Therefore the measured mass scales as $M_* \propto D/\sin^2 i$ (see for example Table 3 in Dutrey et al. 2003). R_{out} (col. 8) is the outer radius of the line emission and M_* is the measured mass (col. 9). For stars with precise distances, uncertainties of the inclination dominate the mass uncertainty. When only the average distance is known, we use the distance-independent parameter L/M^2 to present the results on a modified Hertzsprung–Russell Diagram.

Table 4 gives the observational results for the Akeson-Jensen sample. Its format is identical to Table 3 except it also lists the binary separations (col. 3) as given by AJ14; “S” designates the stars they identified as probably single. A and B denote the primary and secondary. We were able to measure masses of both components for HK Tau, as did Jensen & Akeson (2014) also, and for DK Tau.

Table 4 provides disk inclinations for several stars which AJ14 describe as point sources. AJ14 analyzed the data in the image plane, while we derived disk sizes and orientations by fitting a disk model in the UV plane, fitting

Table 4. Measured Parameters in Akesson& Jensen Sample

ID	Name	sep. arc sec	Dist pc	Lines	V_{LSR} km s^{-1}	i_{line} deg	i_{cont} deg	R_{out} AU	M_* M_{\odot}
Bold identifies stars with small L/M^2 values, see §4.3									
1	FV Tau A	0.70	140	CO	7.30 ± 0.30	81 ± 2	79 ± 7	57 ± 2	2.30 ± 0.17
2	FX Tau A	0.68	140	CO	6.70 ± 0.08	40 ± 4	20 ± 20	40 ± 10	1.70 ± 0.18
3	HBC 411 B	2.8	140	CO	5.50 ± 0.10	25 ± 1		33 ± 2	2.05 ± 0.20
4	CIDA-9 A	2.2	140	CO	6.48 ± 0.01	33 ± 2	34 ± 6	192 ± 2	1.08 ± 0.20
5A	HK Tau A	2.3	140	CO	5.98 ± 0.04	51 ± 2	54 ± 7	90 ± 10	0.58 ± 0.05
5B	HK Tau B		140	CO	6.43 ± 0.05	81 ± 2		120 ± 10	1.00 ± 0.03
6	IT Tau B	2.4	140	CO	6.40 ± 0.30	66 ± 12		50 ± 3	0.50 ± 0.08
7A	DK Tau A	3.4	140	CO	5.57 ± 0.20	20 ± 5	65 ± 8	38 ± 4	0.60 ± 0.14
7B	DK Tau B		140	CO	6.30 ± 0.30	55 ± 10		60 ± 12	1.30 ± 0.30
8	GK Tau	S	131	CO	6.26 ± 0.05	71 ± 5		82 ± 2	0.79 ± 0.07
9	HN Tau A	3.0	140	CO	5.65 ± 0.13	75 ± 4	50 ± 15	52 ± 10	1.57 ± 0.15
10	V710 Tau A	3.2	140	CO	6.64 ± 0.04	46 ± 5	47 ± 4	82 ± 6	0.66 ± 0.06
11	HO Tau	S	161	CO	5.65 ± 0.15	64 ± 3	35 ± 20	62 ± 5	0.37 ± 0.03
12	DS Tau	S	140	CO	5.68 ± 0.02	71 ± 1	69 ± 6	164 ± 2	0.73 ± 0.02

both frequencies simultaneously. We list the masses at 140 pc except for GK Tau and HO Tau as discussed in §2.2. Star names in bold have small values of L/M^2 ; see §4.2 and 5.3 for details. Fig. B10 (in Appendix) shows the disk emission in CO 3-2 towards the observed sources.

4. DERIVED MASSES IN TAURUS AND OPHIUCHUS

4.1. Masses for ALMA Cycle 2 Stars in L1495 and Other Stars with Known Distances

Stars with measured mass to an internal precision smaller than 5% and accurate and precise distances may be considered to have good values of their absolute mass, an intrinsic property of the star. This is the case for the stars in Table 3 and we may analyze them on a conventional Hertzsprung-Russell diagram (HRD). Fig. 4 places the stars on HRDs using the (L, T_{eff}) values of And13 and He14. The figures also include several other stars in Taurus with masses measured to internal precision better than 5% and with reliable distances that we have published previously: the single stars GM Aur, DL Tau, and CI Tau (Guilloteau et al. 2014) and the binary V807 Tau Ba, Bb (Schaefer et al. 2012). Schaefer et al. (2012) used a distance 140 pc for V807 Tau; here we use the 161 pc distance of L1529. The figures use evolutionary models calculated by Baraffe et al. (2015, BHAC15).

More recently, Feiden (2016, F16) published models of PMS evolution that include models with and without internal magnetic fields. It is of interest to apply F16’s non-magnetic models to the stars with well-determined absolute masses. We do this in Fig. 5 for the same stars as in Fig. 4 and use And13’s stellar parameters. Fig. 5 is nearly identical to Fig. 4 (left). The only significant difference is seen in the 1 MY isochrone: stars with mass in the range $\sim 0.2 - 0.5 M_{\odot}$ appear more luminous than in the BHAC15 models. This may be the effect of different treatments of deuterium burning. The effect is to make stars CY Tau, FP Tau, CX Tau, V807 Tau Ba and Bb appear slightly older than the ~ 1 MY indicated in Fig. 4. Given the similarity of the F16 and BHAC15 models we will continue to apply the BHAC15 models to our mass measurements.

The spacing of the evolutionary tracks in Fig. 4 is $0.1 M_{\odot}$. Since this is greater than the precision of the measured masses we can investigate whether the measured mass is consistent with an evolutionary track of corresponding mass. In fact, Fig. 4 shows that the comparison is often limited by uncertainties in T_{eff} . We make a rough assessment of the level of agreement between the absolute mass and the evolutionary track (here BHAC15) as follows and illustrated in Fig. 6 for IP Tau (absolute mass = $0.95 \pm 0.02 M_{\odot}$). We draw an error ellipse centered at the $(\log(T_{\text{eff}}), \log(L/L_{\odot}))$ for each star using the stellar parameters and their uncertainties quoted in Table 3. We estimate the level of agreement by the distance in the HRD plane between the error ellipse and the evolutionary track corresponding to the measured absolute mass. The mass uncertainty is smaller than the filled circle used to plot the position of IP Tau in Fig. 6 and all the stars plotted in Figs. 4-5. We emphasize that the masses in Table 3 are measures of a fundamental property of the stars completely independent of their T_{eff} and L . As such if we find, as we do, that the positions on the HRD of

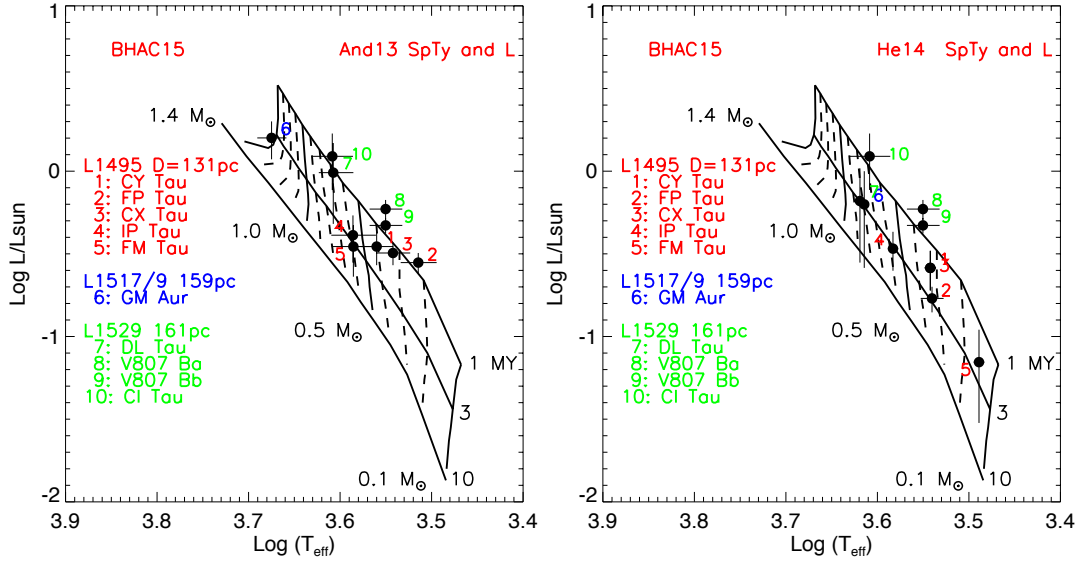


Figure 4. An HRD for single PMS stars in the L1495 region in the Taurus SFR with absolute masses measured dynamically in our ALMA Cycle 2 observations. We include data for stars in L1517 and L1529 in Taurus from Guilloteau et al. 2014 and Schaefer et al. 2012. Left: luminosities and effective temperatures given by Andrews et al. (2013, And13), and right from Herczeg and Hillenbrand (2014, He14). In the right panel, the positions of stars CY Tau (1) and CX Tau (3) are identical.

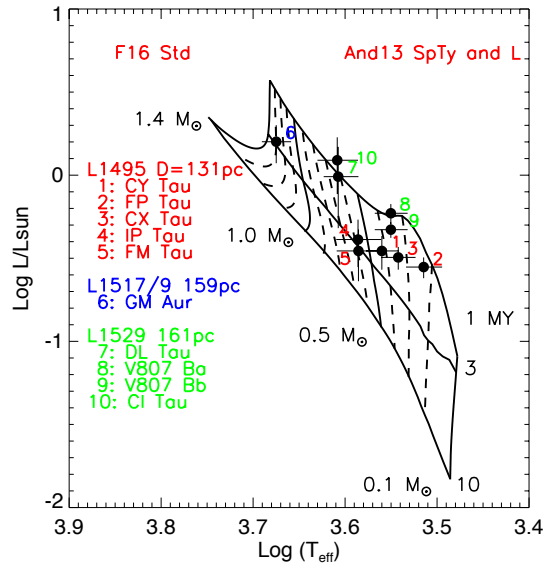


Figure 5. Identical to Fig. 4 except that the HRD uses the non-magnetic evolutionary models calculated by Feiden (2016, F16) and only the luminosities and effective temperatures given by And13.

most of the stars lie close to the evolutionary track corresponding to their measured masses, but some do not, the fault for the discrepant stars lies not with the models but probably mostly with their separately determined T_{eff} s. Their luminosities are less likely at fault because the evolutionary tracks are nearly vertical at young ages. This approach assumes that the tracks have no uncertainty and we return to this point in §5.1. Table 5 summarizes the comparisons and lists the ages indicated.

Fig. 4 shows that masses measured for CY Tau, CX Tau, and CI Tau are consistent to about 1σ with the (L, T_{eff}) values given by And13 and the BHAC15 models at ages 1-3 MY. The relatively large discrepancy for V807 Tau Ba and Bb, is probably attributable to the limited data available to estimate their (L, T_{eff}) (Schaefer et al. 2012). We estimate also in Table 5 the sense of the discrepancy with respect to the spectral type for the star. C indicates that the listed spectral type is too cool and H that it is too hot. In most cases the reported spectral type is too cool, that is, the measured mass would be better represented by a hotter T_{eff} . In the case of IP Tau the discrepancy in T_{eff} could be attributable to the possibility that it is actually a binary. IP Tau’s continuum image (Fig. 1) clearly shows an

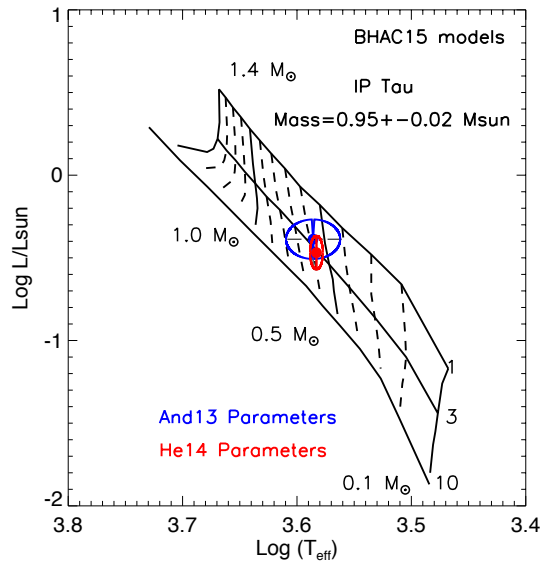


Figure 6. The HRD shows IP Tau plotted at the T_{eff} and L/L_{sun} given by Andrews et al. (2013, And13) (blue) and Herczeg & Hillenbrand (2014) (red) and uses their uncertainties to calculate the uncertainty ellipses. The uncertainty ellipse is used as a unit for measuring the distance between IP Tau’s stellar parameters and the BHAC15 evolutionary track corresponding to its absolute dynamical mass, $0.95 \pm 0.02 M_{\odot}$.

Table 5. Results: Comparison with Tracks in L1495 and L1688

Name	Mass (M_{\odot})	And13	SpTy	Age (MY)	He14	SpTy	Age (MY)
Stars in L1495							
CY Tau	0.31 ± 0.02	$< 1\sigma$	Ok	2	$< 1\sigma$	Ok	2
FP Tau	0.37 ± 0.02	$\sim 2\sigma$	C	1	$< 1\sigma$	Ok	3
CX Tau	0.37 ± 0.02	$< 1\sigma$	Ok	1	$\sim 1\sigma$	Ok	2
IP Tau	0.95 ± 0.02	$\sim 2\sigma$	C	3	$\sim 4\sigma$	C	3
FM Tau	0.36 ± 0.01	$\sim 2\sigma$	H	3	$\sim 5\sigma$	C	2
GM Aur	1.14 ± 0.02	$\sim 2\sigma$	H	3	$\sim 10\sigma$	C	3
DL Tau	1.05 ± 0.02	$\sim 2\sigma$	C	1	$\sim 4\sigma$	C	3
V807 Tau Ba	0.86 ± 0.03	$\sim 5\sigma$	C	< 1	$\sim 5\sigma$	C	< 1
V807 Tau Bb	0.73 ± 0.03	$\sim 4\sigma$	C	1	$\sim 4\sigma$	C	1
CI Tau	0.92 ± 0.02	$\sim 1\sigma$	Ok	3	$\sim 1\sigma$	C	1
Stars in L1688							
Name	Mass (M_{\odot})	R10a	SpTy	Age (MY)			
GSS 26	1.51 ± 0.02	$\sim 5\sigma$	C	1/2			
GSS 39	0.47 ± 0.01	$< 1\sigma$	Ok	1			
YLW 16C	1.80 ± 0.10	$> \sim 10\sigma$	C	1/2			
ROXs 25	1.10 ± 0.07	$< 1\sigma$	Ok	1/2			
YLW 58	0.09 ± 0.01	$< 1\sigma$	Ok	1			

inner cavity. We discuss this possibility further in §5.3. Fig. 4 shows that the comparison with He14’s (L, T_{eff}) values is similar. The measured masses of CY Tau, FP Tau, CX Tau, and CI Tau are consistent with the tracks. The stars’ ages also lie in the range 1-3 MY. That the differences are much greater for FM Tau, GM Aur, and DL Tau, seems attributable to the very small uncertainties He14 assigned to their spectral types.

4.2. Masses for ALMA Cycle 2 - Ophiuchus Stars with Known Distances

Table 3 indicates that the precision of the mass measurements is better than 7% for all but one of the stars; the exception is YLW 58 measured to 11% precision. The measured masses of the stars in L1688 are therefore good estimates of their absolute values and we plot their (L, T_{eff}) values on conventional HRDs in Fig. 7.

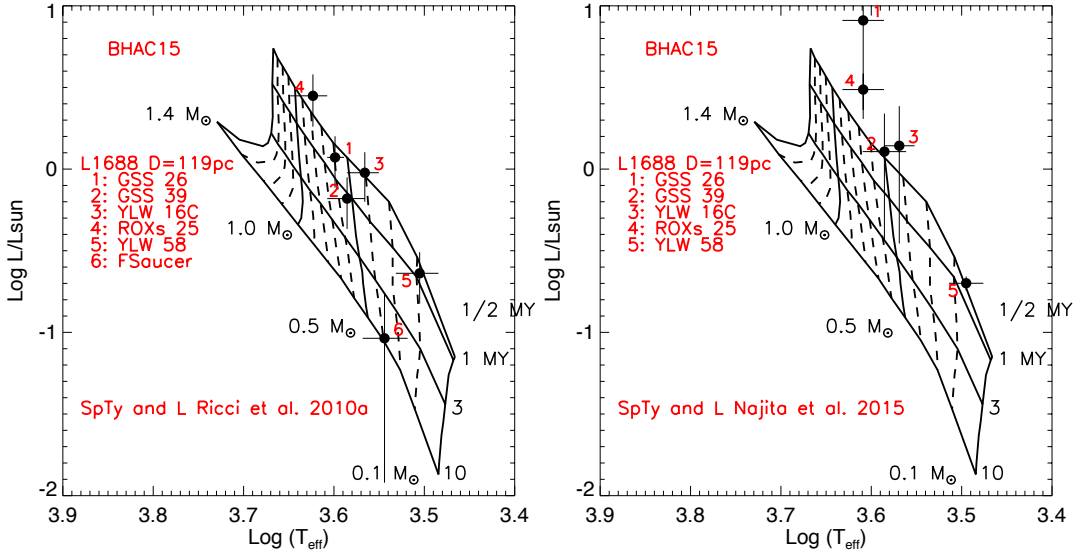


Figure 7. An HRD for single PMS stars in the L1688 of the Ophiuchus SFR with absolute masses measured dynamically in our ALMA Cycle 2 observations. Left: the luminosities and effective temperatures are from Ricci et al. (2010a) for all stars except that the stellar parameters for the Flying Saucer are from Grosso et al. (2003) and Pontoppidan et al. (2007), see text. Right: the luminosities and spectral types are from Najita et al. (2015) (See §4.3).

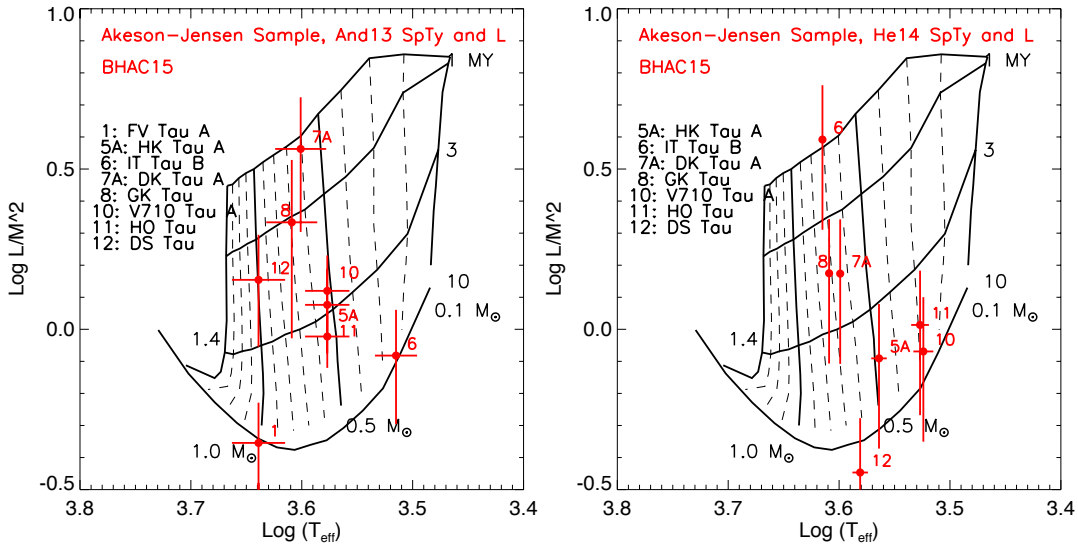


Figure 8. A modified HRD (see §3.2 and 5.1) for components of PMS binaries distributed over the Taurus SFR with masses measured dynamically using Akeson & Jensen’s archived ALMA Cycle 0 observations. Left: luminosities and effective temperatures given by Andrews et al. (2013, And13), right: luminosities and effective temperatures given by Herczeg and Hillenbrand (2014, He14).

Because the spectral types reported by R10a and Najita et al. (2015) are identical or nearly so, the plotted positions of the stars along the T_{eff} axis are nearly the same in both panels of Fig. 7. Their differing positions in the two figures are attributable to different luminosities given by R10a and Najita et al. (2015). The evolutionary tracks at the masses and ages of interest here, are nearly vertical. The luminosity differences therefore correspond to differences in ages. Comparing Figs. 4 and 5 with Fig. 7 it is clear that the stars in L1688 are younger than those in the Taurus SFR with ages less than 1 MY.

Table 5 assesses the positions of the stars in the L1688 with respect to the HRD in Fig. 7. We make the comparisons with the L, T_{eff} values given by R10a because the luminosities given by Najita et al. (2015) indicates ages < 0.5 MY; models for stars this young are uncertain and are not given by BHAC15.

4.3. Masses for ALMA Cycle 0 Stars with Average Association Distance

Table 6. ALMA Cycle 0 Results: Comparison with Tracks and Age Estimates

Name	Mass (M_{\odot})	And13	SpTy	Age (MY)	He14	SpTy	Age (MY)
HK Tau A	0.58 ± 0.05	$< 1\sigma$	Ok	3	$> 3\sigma$	C	2
IT Tau B	0.50 ± 0.08	$\sim 3\sigma$	C	10	$> 3\sigma$	H	< 0.5
GK Tau	0.79 ± 0.07	1σ	Ok	1	$\sim 3\sigma$	C	2
V710 Tau A	0.66 ± 0.06	1σ	Ok	3	$\sim 3\sigma$	C	8
HO Tau	0.37 ± 0.03	$\sim 2\sigma$	H	5	$\sim 2\sigma$	C	7
DS Tau	0.73 ± 0.02	$\sim 2\sigma$	H	2	$\sim 2\sigma$	C	> 10

All the masses in Table 4 are measured to an internal precision better than 25% and 5 are measured to better than 10%. Of the 9 binaries in Table 4, we were able to measure the masses of both components only for HK Tau and DK Tau. Our derived masses for HK Tau A and B improve on the initial determination from Jensen & Akeson (2014)’s. The measured value of the inclination of B’s disk, $i_{line} = 84 \pm 2^{\circ}$, is in excellent agreement with McCabe et al. (2011) value determined from high resolution IR images. We also derive a new value for the inclination of A’s disk, $i_{A,line} = 51 \pm 2^{\circ}$, improving on the original determination of Jensen & Akeson (2014), $43 \pm 5^{\circ}$. We discuss this further in Appendix B. The new values do not affect Jensen&Akeson’s finding that the A and B disks are not co-planar, although the misalignment can be somewhat smaller. For DK Tau A, the difference in inclinations measured in the continuum and line emission is 45° . DK Tau A has a small disk (col. 9) and a solution with $i_{line} \sim 70^{\circ}$ is also possible. This would however imply an unacceptably low mass of $\sim 0.15M_{\odot}$, which would be completely inconsistent with its late K spectral type (Table 2). Higher spatial and spectral observations are needed for DK Tau A.

Because most of the stars in the Akeson-Jensen sample do not have precise distances, we plot them on modified HRDs in which the variable along the abscissa is the distance independent parameter L/M^2 . As in the conventional HRD, a star’s vertical position in the modified HRD measures its age with respect to model isochrones. The measured masses in Table 4 are evaluated at 140 pc (except for GK Tau and HO Tau). Their actual values may differ by $\pm \sim 14\%$ reflecting the dependance of the measured mass on distance and the known spread of distances, $\pm \sim 20$ pc of members of the Taurus SFR.

Fig. 8 uses the stellar parameters of And13 and He14. Of the 14 stars in Table 4, six (FX Tau A, HBC 411 B, CIDA-9 A, HK Tau B, DK Tau B, HN Tau A) do not appear in Fig. 8 (left) because their L/M^2 values are too small, which, taken at face value would imply unreasonably great ages $\gg 10$ MY. The same 6 stars and also a 7th, FV Tau A, do not appear in Fig. 8 (right). In fact, in Fig. 8 (left), FV Tau A falls on the 10 MY isochrone, an age that is suspect given the younger ages of the other stars. We consider the 7 stars with small values of L/M^2 together and identify them in bold in Table 4. We discuss these stars further in §5.3.

Table 6 provides an assessment of the parameters of the stars plotted in Fig. 8 as measured with respect to the BHAC15 evolutionary models in the same format as Table 5. We omit DK Tau A because of the difference in its inclination as measured in the continuum and lines. The number of stars whose spectral type is too cool with respect to the evolutionary track corresponding to its mass is somewhat greater than the number that is too hot, similar to the situation in L1495 and L1688 described in Table 5. Also, there is a greater dispersion in ages among the stars in Table 6. Both effects could be the result of the technical difficulties of measuring spectral types and luminosities in binaries. The measured masses of two stars, GK Tau and HO Tau, are absolute because their distances are provided by association with L1495 and L1529, respectively. They lie within ~ 1 and $\sim 2\sigma$ of the tracks indicated by their mass and their ages are ~ 1 and ~ 5 MY, respectively. We made no entry for FV Tau A because its L/M^2 is anomalously small.

5. DISCUSSION

5.1. Comparison of Measured Masses and Evolutionary tracks on the HRD

Tables 5 and 6 assess the measured stellar masses and effective temperatures with respect to the evolutionary tracks and present estimates of the stellar ages. This information is summarized in Table 7 for stars with and without known distance. For the stars in Taurus, Table 7 extracts assessments using And13’s parameters only. The assessments using He14’s parameters are similar but with greater discrepancies owing to their very small uncertainties on T_{eff} . For the stars in Ophiuchus, we made assessments with respect to Ricci et al. (2010a)’s parameters. Table 7 includes 4 stars DM Tau, LkCa15, GO Tau and IQ Tau whose parameters are reported in Guilloteau et al. (2014). Their masses are measured to an internal precision $< 5\%$ but, because the distances to the groups in which they lie are unknown

Table 7. Assessment of M_* , L , T_{eff} and Models

Dynamical masses are given in parentheses			
Known Distance		Average Distance	
Agreement $\leq 1\sigma$	$\leq 2\sigma$	Agreement $\leq 1\sigma$	$\leq 2\sigma$
YLW 58 (0.09)	FM Tau (0.36)	DM Tau (0.53)	GO Tau (0.48)
CY Tau (0.31)	FP Tau (0.37)	V710 Tau A (0.66)	DS Tau (0.73)
CX Tau (0.37)	HO Tau (0.37)	LkCa15 (1.01)	IQ Tau (0.79)
GSS 39 (0.47)	GM Aur (1.14)	HK Tau A (0.58)	
GK Tau (0.79)	IP Tau (0.95)		
CI Tau (0.92)			
DL Tau (1.05)			
ROXs 25 (1.10)			

the masses are evaluated at 140pc. We estimated their separation in the $(L/M^2, T_{\text{eff}})$ from the evolutionary track corresponding to their mass in the same manner as in Tables 5 and 6 (e.g. Fig. 7 in [Guilloteau et al. 2014](#)). The evolutionary tracks used in [Guilloteau et al. \(2014\)](#) are essentially F16 non-magnetic tracks which in the mass range of these stars is very similar to those of BHAC15 (see §4.1 and Fig. 5).

The stars with known distance are listed in Cols. 1 and 2 of Table 7. These masses are model independent in that they depend only on the interferometric observations and the cluster distances. Thus, the masses in Cols. 1 and 2 are absolute, that is, an intrinsic property of the stars. All have mass precisions $< 11\%$ and most $< 6\%$. Cols. 1 and 2 list the stars which lie within 1σ and 2σ , respectively, of the evolutionary tracks corresponding to their mass. The measured mass is indicated in parentheses. For the stars in Col. 1, it is truly significant that the PMS evolutionary tracks and the measured absolute masses and T_{eff} s are consistent to 1σ in the range 0.09 to 1.1 M_{\odot} and at ages < 3 MY.

The stars in cols. 3 and 4 have mass measured to an internal precision 10% or better. When accurate and sufficiently precise *GAIA* parallaxes for these stars become available, their masses will become absolute. These stars will then enable further tests of the evolutionary models. Columns 3 and 4 include stars with L/M^2 large enough (ages sufficiently young) to appear in Fig. 8. We discuss in §5.3 the stars with L/M^2 too small to appear in Fig. 8.

Where do the problems lie when there is a discrepancy of the stellar parameters with respect to the evolutionary tracks? Do they lie with the measured mass, luminosity, spectral type, and hence effective temperature, and/or the evolutionary models? That the BHAC15 and F16's non-magnetic models agree well gives us confidence that they are a good starting point for the evaluation of our results.

Discrepancy in the HRD position of a star can be attributed either to its measured mass or spectral type and hence T_{eff} . The luminosity does not enter because a young star contracts at almost constant T_{eff} . Uncertainty in luminosity produces an age uncertainty. We are confident of the mass measurements of the stars in cols. 1 and 3 because their disks are positioned such that their inclinations are not small and are sufficiently extensive that we were able to measure the inclinations and rotation accurately. This suggests that the departure of a star's T_{eff} from the model value is responsible for the discrepancy. These departures include the aleatory parameters that can vary from star to star according to its circumstances determined by chance. These include the accretion luminosity, stellar activity, starspots and their time variation.

5.2. Ages in Taurus and Ophiuchus SFRs

Most of the stars in Taurus considered here have ages in the range 1 to 3 MY. Although the luminosity uncertainties for the very obscured stars in L1688 can be very much greater than for the less obscured stars in Taurus, all the stars in Fig. 7 except the Flying Saucer indicate an age younger than 1 MY. Because the uncertainty of the Flying Saucer's luminosity is especially large and its spectral type uncertain, we regard its present position on the HRD as preliminary. That the stars in L1688 are younger than those in L1495 supports the finding that the Ophiuchus SFR is younger than the Taurus SFR ([Kenyon et al. 2008](#); [Wilking et al. 2008](#)).

These estimated ages are based on the BHAC15 models that do not include the effects of internal magnetic fields. F16 and [MacDonald & Mullan \(2017\)](#) showed that the pressure of magnetic fields included in the convective regions of PMS stars slows their contraction. Thus, given a star's luminosity and effective temperature, the star will appear older when magnetic effects are considered. The effect on estimated age is mass dependent and a full analysis

will have to await a larger sample of measured masses than presently available.

5.3. Stars with Small L/M^2 Values

The L/M^2 values of 7 stars identified in bold in Table 4 are so small that they imply ages unrealistically large for members of the Taurus SFR. They can be smaller than expected either because their masses are large or because their luminosities are small for their mass, or both. Two characteristics of this sample stand out. Their masses are all greater than the masses of those that do appear in Fig. 8; all are greater than $1 M_{\odot}$ while the largest mass of the plotted stars is $0.79 \pm 0.07 M_{\odot}$. Binary separations may also play a role but a lesser one. The components of two binaries with the smallest separations, FV Tau and FX Tau, $< 1''$, have small L/M^2 values while three of the stars that AJ14 found are singles, GK Tau, HO Tau, and DS Tau, appear in Fig. 8. However, other stars in both groups are in binaries that have separations $> 2''$ indicating that more is involved than binarity.

It is not possible that FV Tau A ($2.3 M_{\odot}$), HBC411 B ($2.07 M_{\odot}$), and FX Tau A ($1.7 M_{\odot}$) are single stars because their luminosities are too small and T_{eff} s are too cool for stars of such masses. It seems likely that the stars with small L/M^2 values are actually unresolved binaries or higher order multiples themselves. With the evolutionary models as a guide we find that it is possible to account for the (L, T_{eff}) of the stars with low L/M^2 values as unresolved multiples of lower mass stars. The details of the possible composite systems depend on whether the And13 or He14 parameters are used. Observations that can identify the hypothetical components by either radial velocity measurements or interferometric imaging will elucidate the nature of these stars.

Further evidence for a higher multiplicity as the main cause of discrepancy between spectral types and dynamical masses is provided by IP Tau, MHO 2, and YLW 16c. We drew attention (§4.1) to the cavity detected at the center of IP Tau’s continuum image. Using its measured mass and luminosity (either the And13 or He14 values) we find that its L/M^2 and T_{eff} values would place it on or below the 10 MY isochrones on modified HRDs such as those in Fig. 6. As for the other stars with small L/M^2 values, this supports the possibility that IP Tau is an unresolved binary. The finding of a third component in the GG Tau Aa, Ab binary (DiFolco et al. 2014), namely that Ab is itself a close binary Ab1 and Ab2, is an example of components yet to be found. MHO 2 is surrounded by a striking circumbinary ring of dust emission (Fig. 1), from which an accurate orientation and inclination can be derived. CO J=2-1 emission is also detected, but strong confusion with the molecular cloud limits our ability to measure the dynamical mass (see Fig. B8). Yet, the presence of emission at sufficiently high velocities rule out very low mass: allowed values are in the range $0.5 - 0.8 M_{\odot}$, while the spectral type is M2.5 (Briceño et al. 1998). The measured mass of YLW16C, $1.80 \pm 0.10 M_{\odot}$ draws attention because it is the highest of those we measured in L1688 and its T_{eff} is too low for its mass. Its L/M^2 and T_{eff} would also place it below a 10 MY isochrone in the modified HRD. It seems likely that YLW16C is an unresolved binary too.

5.4. Spectral lines from Disks

A very serious obstacle for mass determination by the rotation of the host star’s circumstellar disk is contamination of the disk line emission by molecular clouds along the line of sight. To overcome this, we tested the detectability of the hyperfine-split CN 2-1 transition radiated by circumstellar disks. We found that the CN lines were good tracers of disk emission of targets in the Taurus SFR and were free of molecular absorption (Guilloteau et al. 2013). We then used the Plateau de Bure interferometer to measure the masses of 11 stars in the Taurus SFR (Guilloteau et al. 2014). However, Reboussin et al. (2015) showed that CN line emission from disks was more difficult to detect in the ρ Oph region than in the Taurus SFR. Smaller disks, perhaps because of the much denser environment of L1688, different chemistry because of the younger ages were suggested as possible causes for this difference.

L1688 is significantly different from L1495 in at least two respects. The number and number density of stars in L1688 is greater than in L1495 (Wilking et al. 2008; McClure et al. 2010; Kenyon et al. 2008). Using their counts of stars and maps of the two regions, the stellar density is 45 stars pc^{-3} and $0.27 \text{ stars pc}^{-3}$ in L1688 and L1495 respectively. The greater extinction to the stars in L1688 than in L1495 indicates that the density of interstellar material also is greater (McClure et al. 2010; And13; He14). The different environments to which the disks are exposed may affect the abundances of CN in ways not yet explored.

Anticipating that the stars we planned to observed in L1688 would suffer strong line of sight contamination in CO J=2-1, our strategy with ALMA was to observe simultaneously in the CN 2-1 transitions and the CO 2-1 and H_2CO lines. Most disks in our sample were found to be smaller than those in the Guilloteau et al. (2013) sample. However, this is probably a selection bias: the targets of our ALMA study have T_{eff} s cooler than the stars in our pilot studies (Guilloteau et al. 2013, 2014). Indeed, there is no difference in disk size in our new sample between the L1495 and L1688 regions. Nevertheless, CN is detectable in most sources in the L1688 region, but the N=2-1 line

emission is heavily contaminated by apparent absorption from the molecular cloud, except for the Flying Saucer which lies in the outskirts of the region. The apparent absorption is partly due to filtering of the extended emission by the interferometer, but true absorption against the strong continuum of some disks may also occur. The intensity ratio of the hyperfine components indicates that the CN line from the molecular cloud has moderate optical thickness. A similar contamination is seen towards MHO 1-2 in the Taurus SFR. In other Taurus sources, CN is barely detectable because of the limited brightness sensitivity of the observations, a result of observing with longer baselines than initially requested in the proposal.

Contamination in H_2CO is much less significant than in CN, but still detectable in L1688. In practice, the precision of our mass measurements relies mostly on the higher signal to noise obtained with the CO J=2-1 transition, but the other lines nevertheless play a key role in allowing a more accurate measurement of the systemic velocity.

6. SUMMARY

1) Our ALMA Cycle 2 program has yielded absolute dynamical masses for 5 stars in L1495 and 6 in L1688. 7 of these are at masses $< 0.6 M_\odot$, and of these 6 are at precision $< 5\%$.

2) We find good agreement with the measured parameters of 8 stars with the BHAC15 and F16 evolutionary models over the mass range ~ 0.09 to $1.10 M_\odot$. It seems reasonable to attribute the lesser agreement of 5 stars to the aleatory properties of PMS stars that can affect the T_{eff} measurement.

3) Positions on the HRD with respect to the isochrones of the BHAC15 models indicate the stars we observed in three Lynds clouds in Taurus have age 1 to 3 MY and those in L1688 in Ophiuchus with reliable luminosities are younger than 1 MY.

4) We also measured masses of 14 stars in the ALMA Cycle 0 archival data for Akeson and Jensen's (2014, AJ14) study of disks associated with binaries in Taurus. Most of the measured masses are greater than those in our Cycle 2 program. We confirm AJ14's measurement of the masses of HK Tau A and B.

5) The masses measured for 7 targets in the AJ14 sample are sufficiently large as to be inconsistent with their T_{eff} s and luminosities. The most plausible explanation is that these components are actually binaries or higher order multiples. Similar considerations suggest that IP Tau and YLW 16c in our ALMA sample may also be unresolved binaries.

6) We detected strong contamination of disk emission in CN lines by the molecular cloud in L1688, and towards MHO 1-2 in L1495. H_2CO is less affected, but fainter. Dynamical mass measurements in dense regions will require a combination of spectral lines with different opacities to overcome the contamination on one hand, and the sensitivity limitation on the other hand.

Facility: ALMA.

We thank the referee for a thorough reading of our paper and comments that improved the presentation. We thank R. Akeson and E. Jensen for their interest in having us re-analyze their Cycle 0 data. We are grateful to I. Baraffe, G. Feiden, G. Herczeg, J. Najita and L. Ricci for their quick and thorough replies to our questions and especially to M. McClure for a thorough assessment of the luminosity uncertainties in L1688. MS thanks J. Toraskar for help with the HRD plots.

This paper makes use of the following ALMA data: ADS/JAO.ALMA#2011.0.00150.S, ADS/JAO.ALMA#2013.2.00163.S and ADS/JAO.ALMA#2013.2.00426.S. ALMA is a partnership of ESO (representing its member states), NSF (USA) and NINS (Japan), together with NRC (Canada) and NSC and ASIAA (Taiwan), in cooperation with the Republic of Chile. The Joint ALMA Observatory is operated by ESO, AUI/NRAO and NAOJ. This research made use of the SIMBAD database, operated at CDS, Strasbourg, France. This research was supported by the "Programme National de Physique Stellaire" and the "Action Spécifique ALMA" of INSU/CNRS (France).

REFERENCES

- | | |
|--|---|
| Akeson, R. L., & Jensen, E. L. N. 2014, ApJ, 784, 62 | Baraffe, I., Homeier, D., Allard, F., & Chabrier, G. 2015, A&A, 577, A42 |
| Allard, F., Homeier, D., & Freytag, B. 2012, Philosophical Transactions of the Royal Society of London Series A, 370, 2765 | Briceño, C., Hartmann, L., Stauffer, J., & Martín, E. 1998, AJ, 115, 2074 |
| Andrews, S. M., Rosenfeld, K. A., Kraus, A. L., & Wilner, D. J. 2013, ApJ, 771, 129 | Dame, T. M., Hartmann, D., & Thaddeus, P. 2001, ApJ, 547, 792 |
| | Dartois, E., Dutrey, A., & Guilloteau, S. 2003, A&A, 399, 773 |

- Di Folco, E., Dutrey, A., Le Bouquin, J. B., S., et al. 2014A&A, 565, 2
- Dutrey, A., Guilloteau, S., & Simon, M. 2003, A&A, 402, 1003
- Feiden, G. A. 2016, A&A, 593, A99
- Grosso, N., Alves, J., Wood, K., et al. 2003, ApJ, 586, 296
- Guilloteau, S., Di Folco, E., Dutrey, A., et al. 2013, A&A, 549, A92
- Guilloteau, S., Simon, M., Piétu, V., et al. 2014, A&A, 567, A117
- Guilloteau, S., Reboussin, L., Dutrey, A., et al. 2016, A&A, 592, A124
- Herczeg, G. J., & Hillenbrand, L. A. 2014, ApJ, 786, 97
- Jensen, E. L. N., & Akeson, R. 2014, Nature, 511, 567
- Kenyon, S. J., Gómez, M., & Whitney, B. A. 2008, Low Mass Star Formation in the Taurus-Auriga Clouds, ed. B. Reipurth, 405
- Kurucz, R. L. 1979, ApJS, 40, 1
- Loinard, L., Torres, R. M., Mioduszewski, A. J., & Rodríguez, L. F. 2008, ApJL, 675, L29
- Lynds, B. T. 1962, ApJS, 7, 1
- MacDonald, J., & Mullan, D. J. 2017, ApJ, 834, 67
- McCabe, C., Duchêne, G., Pinte, C., et al. 2011, ApJ, 727, 90
- McClure, M. K., Furlan, E., Manoj, P., et al. 2010, ApJS, 188, 75
- McClure, R. J., Dunlop, J. S., Cirasuolo, M., et al. 2010, MNRAS, 403, 960
- Najita, J. R., Andrews, S. M., & Muzerolle, J. 2015, MNRAS, 450, 3559
- Pecaut, M. J., & Mamajek, E. E. 2013, ApJS, 208, 9
- Piétu, V., Dutrey, A., & Guilloteau, S. 2007, A&A, 467, 163
- Piétu, V., Guilloteau, S., Di Folco, E., Dutrey, A., & Boehler, Y. 2014, A&A, 564, A95
- Pinte, C., Dent, W. R. F., Ménard, F., et al. 2016, ApJ, 816, 25
- Pontoppidan, K. M., Stapelfeldt, K. R., Blake, G. A., van Dishoeck, E. F., & Dullemond, C. P. 2007, ApJL, 658, L111
- Reboussin, L., Guilloteau, S., Simon, M., et al. 2015, A&A, 578, A31
- Ricci, L., Testi, L., Natta, A., & Brooks, K. J. 2010a, A&A, 521, A66
- Ricci, L., Testi, L., Natta, A., et al. 2010b, A&A, 512, A15
- Schaefer, G. H., Prato, L., Simon, M., & Zavala, R. T. 2012, ApJ, 756, 120
- Torres, R. M., Loinard, L., Mioduszewski, A. J., et al. 2012, ApJ, 747, 18
- Torres, R. M., Loinard, L., Mioduszewski, A. J., & Rodríguez, L. F. 2009, ApJ, 698, 242
- Wilking, B. A., Gagné, M., & Allen, L. E. 2008, Star Formation in the ρ Ophiuchi Molecular Cloud, ed. B. Reipurth, 351

APPENDIX

A. METHOD OF ANALYSIS

We use the *DiskFit* tool (Piétu et al. 2007) to derive the disk properties by fitting truncated power law disk models. The disk model is that of a flared disk with power laws for the temperature ($T(r) = T_0(r/R_0)^{-q}$), surface density ($\Sigma(r) = \Sigma_0(r/R_0)^{-p}$) and scale height ($H(r) = H_0(r/R_0)^{-h}$) radial distributions, and sharp inner (R_{in}) and outer (R_{out}) radii. The emission from the disk is computed using a ray-tracing method. For spectral lines, we assume that the velocity field is Keplerian, $v(r) = V_0(r/R_0)^{-0.5}$ and use a constant local linewidth δV . Besides the above disk parameters, 4 geometric parameters are required to derive the disk emission: the disk position (x_0, y_0), orientation PA and inclination i , plus the systemic velocity V_{sys} for spectral lines.

The χ^2 difference between the predicted model visibilities (using the uv coverage from the observations) and the observed ones is minimized using a modified Levenberg-Marquardt method, and the errorbars are derived from the covariance matrix. In practice, R_{in} is set to a small value (0.1 au), and the scale height is kept fixed in the process.

In this analysis, we are only interested in recovering the rotation velocity V_0 at R_0 from which we derive the stellar mass $M_* = R_0 V_0^2 / G$, where G is the gravitational constant. The validity of the errorbars was further assessed by running Monte Carlo Markov Chain (MCMC) in several cases and comparing their results to the simpler minimization method. The agreement is in general excellent because most parameters are only loosely coupled. Apart from the strong coupling between V_0 and $\sin(i)$, since only the projected velocity is measured, the MCMC only revealed a weak coupling between V_{sys} and V_0 .

This weak coupling is not insignificant because contamination by the foreground (or background) cloud emission prevents using a fraction of the available velocities, especially in the CO J=2-1 line. Contaminated velocities are ignored in our minimization process. However, in some cases (e.g. GSS 39), only one wing of the overall velocity spread of the disk can be seen, leaving a substantial uncertainty for V_{sys} . We mitigated these problems by using the velocities derived from the CN or H₂CO lines, if bright enough (e.g. in the Flying Saucer or GSS 39). We also ensured that the results did not depend critically on the masked velocity range.

The reliability of our measurements is confirmed in several ways. First, repeated observations (e.g. CX Tau observed in two ALMA projects) yield consistent results. Second, when more than one spectral line is useable, the results also agree (e.g. CO J=2-1 and CO J=3-2 in CX Tau, or CN and H₂CO in the Flying Saucer). Most importantly, consistent inclinations and orientations are derived from the continuum and the spectral line data. DK Tau A is an exception attributable to its small disk; see §4.3 for discussion. This is significant because these two types of observations are limited by different problems: the continuum data is affected by residual phase and amplitude calibration errors, while the line data is affected by bandpass calibration errors. Furthermore, the disk sizes are quite different in line and continuum, so that any bias due to an inappropriate disk model should have a different impact.

We also expect dust to be settled towards the disk mid-plane, as found for example in the Flying Saucer by [Guilloteau et al. \(2016\)](#) and HL Tau by [Pinte et al. 2016](#)). Molecules, however, sample different heights above the disk mid-plane. The agreement between the inclinations derived in different ways show that these structural differences do not dominate the current errors on the inclination.

The masses of a few sources had already been derived before. [Piétu et al. \(2014\)](#) reported a mass of 0.77 ± 0.07 for DS Tau (at 140 pc) from ^{13}CO J=2-1 observations with the IRAM array, in perfect agreement with our new result. However, for CY Tau [Guilloteau et al. \(2014\)](#) cited a most likely mass of $0.48 M_{\odot}$ (after correction for the 131 pc distance), but the measurement was hampered by ambiguities in the inclination determination because of insufficient angular resolution. The much higher angular resolution used gives an inclination of 30° and yields a lower mass.

B. HK TAU

HK Tau was analyzed by [Jensen & Akeson \(2014\)](#). Overall, we find similar results, but with improved uncertainties. Our analysis differs from theirs in several points. [Jensen & Akeson \(2014\)](#) adjusted an 8 parameter disk model, comprising PA and i , 3 parameters characterizing the CO surface density (using a viscous disk model shape), 2 parameters for the temperature, and the last one is the stellar mass. The disk is in hydrostatic equilibrium, with a constant CO abundance. They assumed that both stars have the same systemic velocity, and fix the positions from the centroid of the velocity integrated CO emission. The orientation and inclination of HK Tau B were taken from optical images. A model of the HK Tau B disk is first subtracted from the data before a model of HK Tau A is fit to the residual. [Jensen & Akeson \(2014\)](#) only used velocities between 0.3-5.4 and 7.9-11.3 km s^{-1} , ignoring the faint wings at higher velocities.

It is possible that the centroid of the CO emission derived by [Jensen & Akeson \(2014\)](#) is biased because of contamination at the surrounding molecular cloud velocity. Furthermore, in an optically thick disk (as expected for CO), the disk flaring produces an asymmetric emission because of the radial temperature gradient ([Dartois et al. 2003](#)), so that the centroid of emission is not on the disk center, but offset along the projected minor axis. Combined with the assumption on velocities, this may have biased the derived inclination and stellar masses.

To evaluate the possible biases, we use a similar, but more complete approach of separate disk fitting. We fitted one disk at a time, and checked that the results did not depend whether the fit used the residual from the other star disk fit, or the whole original data set. We improved on AJ14 analysis by running MCMC chains using either the J=2-1 or the J=3-2 line, or both. Furthermore, our model uses a more comprehensive set of parameters, in particular leaving the positions and systemic velocity as free parameters. We actually find different systemic velocities for both stars. Our derived inclination and orientations for HK Tau B is quite consistent with the optical results, and the two independent determinations (CO J=3-2 and CO J=2-1) of the orientation and inclination of HK Tau A yield consistent results (the continuum at 345 GHz is not sufficiently resolved for this purpose).

Our derived inclination of $51 \pm 2^{\circ}$ is slightly higher than found by [Jensen & Akeson \(2014\)](#). Interestingly, we found that the derived inclination was dependent on the sharpness of the surface density profile. The above value is for steep profiles (the power law exponent of the surface density being $p = 7$, essentially a sharp-edge disk), while for exponents $p < 4$, there is another solution for the inclination, $i \approx 65^{\circ}$. The derived stellar mass remains unaffected, however. Furthermore, this does not affect the main conclusion of [Jensen & Akeson \(2014\)](#) on the mis-alignment, which only drops down to 52 or 58° in the most extreme case instead of 60 or 68° , the two values depending on which side of the HK Tau A disk is closest to us.

The disk around HK Tau A is smaller than that of HK Tau B, as would be expected if caused by tidal truncation because of the stellar mass difference. Interpreting the disk sizes as due to tidal truncation then implies a semi-major axis of about 300-400 au for the orbit, close to the projected separation of 300 au. However, the measured velocity difference is only 0.45 km s^{-1} , inconsistent with a circular orbit. A significant orbital eccentricity would be required to explain the disk sizes by tidal truncation.

Fig. Set 3. Images and integrated spectra of the detected sources.

Fig. Set B10. CO J=3-2 from Akeson & Jensen source sample.

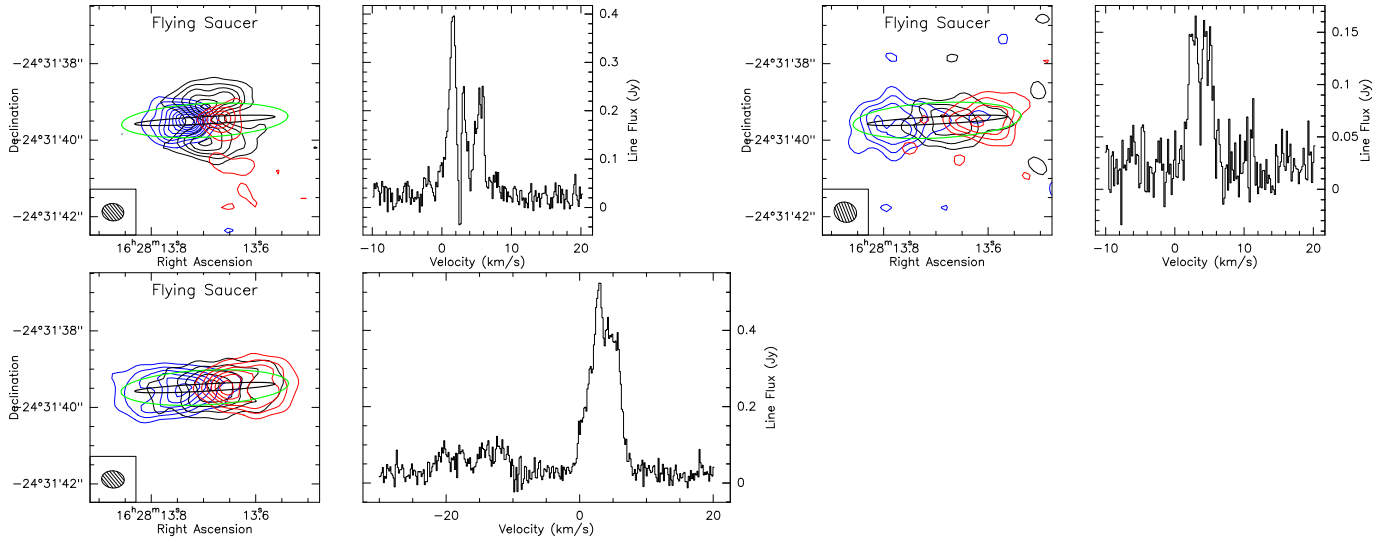


Figure B1. As Fig.3 for the Flying Saucer: CO (top left), H₂CO (top right), CN (bottom).

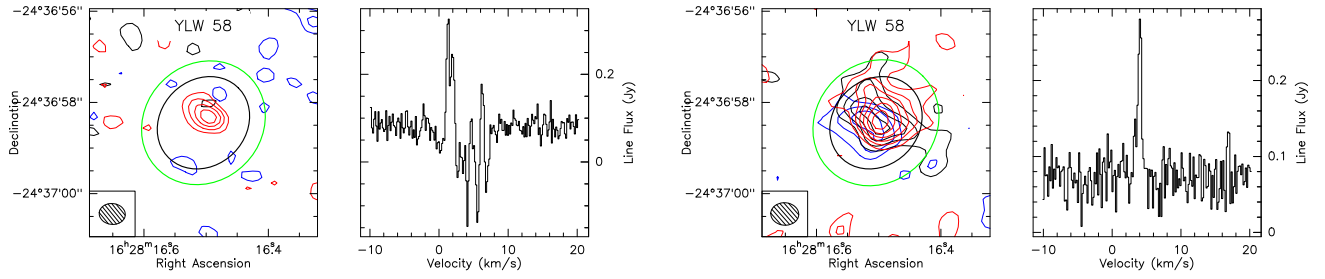


Figure B2. Molecules towards YLW 58: CO (left), H₂CO (right).

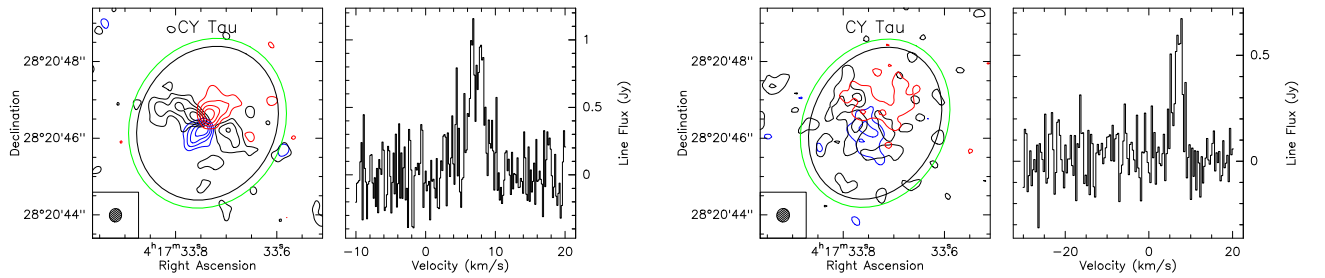


Figure B3. Molecules towards CY Tau: CO (left), CN (right).

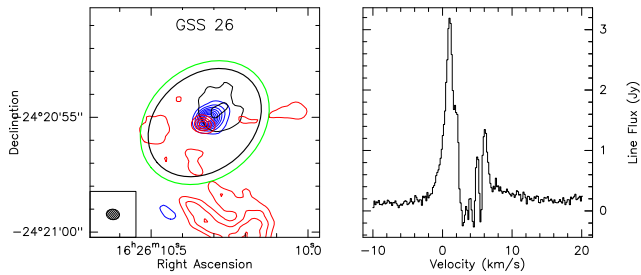


Figure B4. Disk emission in CO J=2-1 of GSS 26.

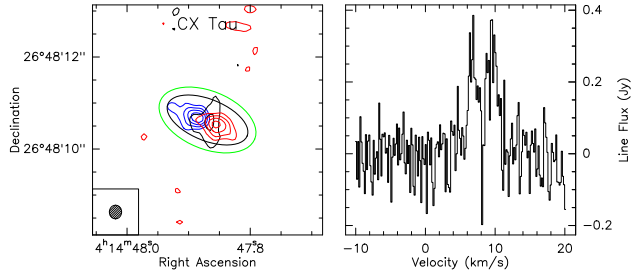


Figure B5. Disk emission in CO J=2-1 of CX Tau.

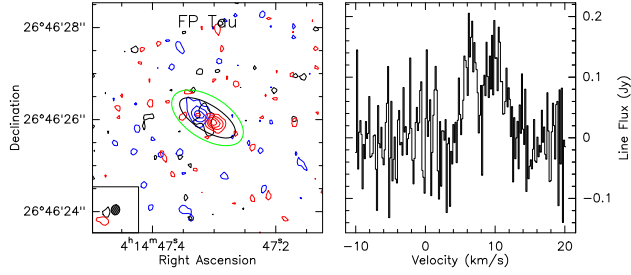


Figure B6. Disk emission in CO J=2-1 of FP Tau.

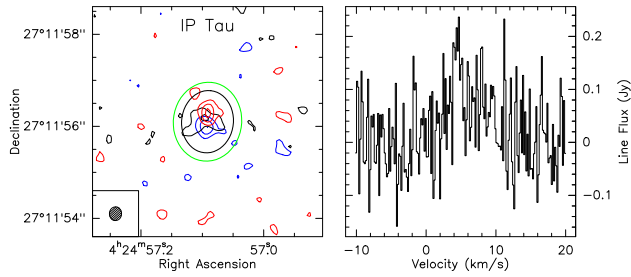


Figure B7. Disk emission in CO J=2-1 of IP Tau.

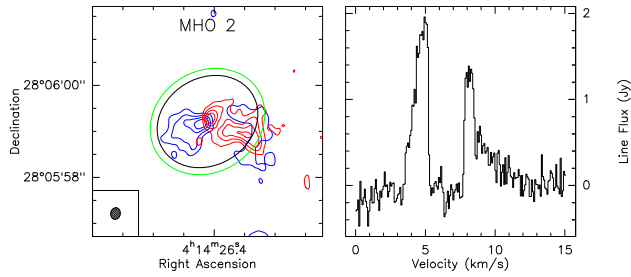


Figure B8. Disk emission in CO J=2-1 of MHO 2.

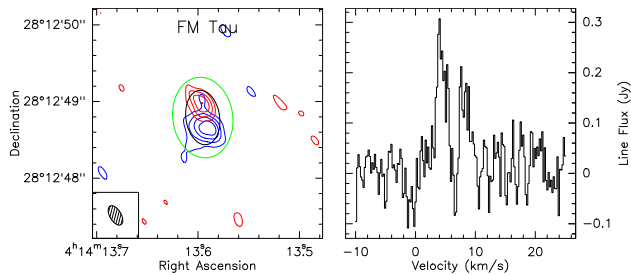


Figure B9. Disk emission in CO J=3-2 of FM Tau.

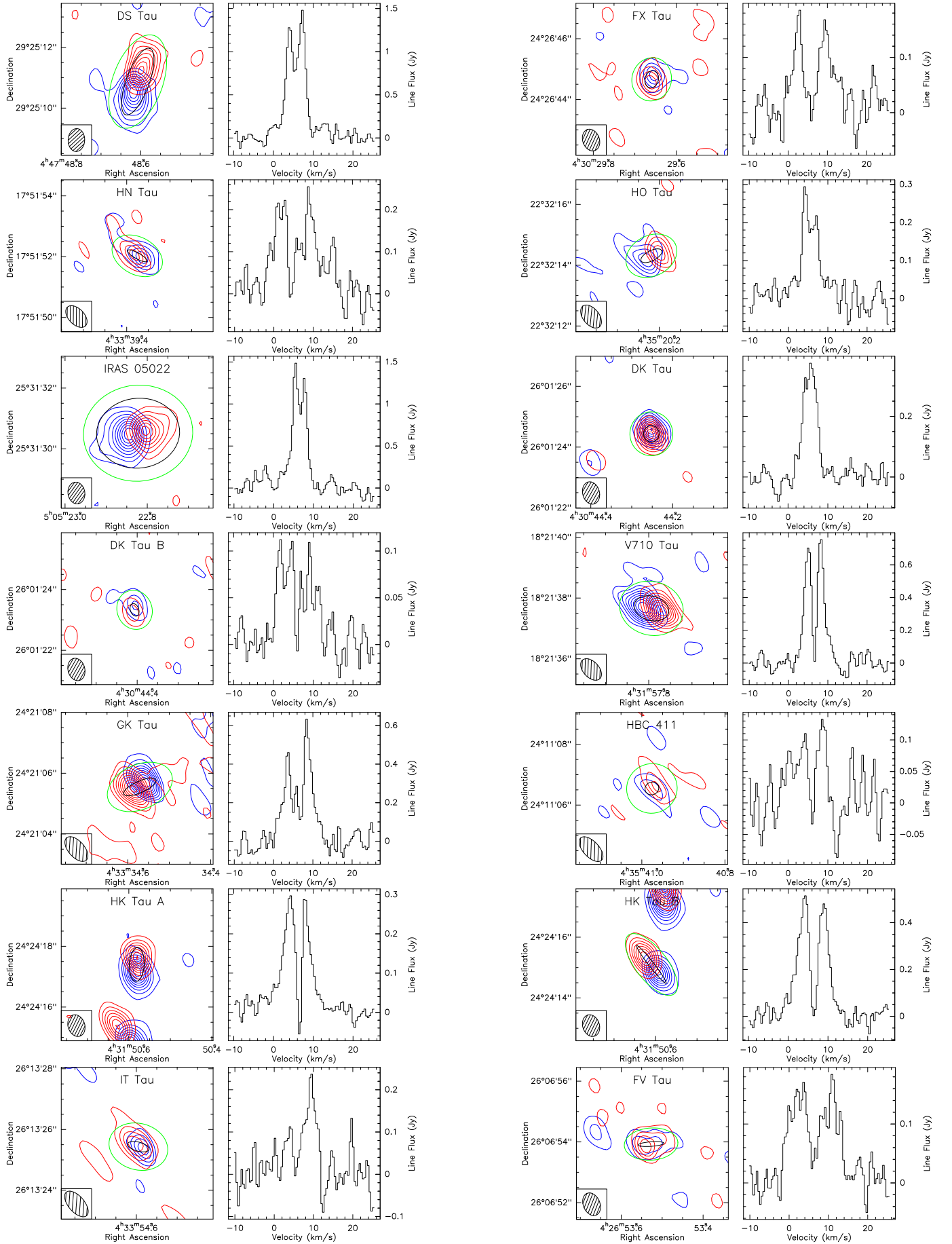


Figure B10. CO J=3-2 from Akeson & Jensen 2014 sample

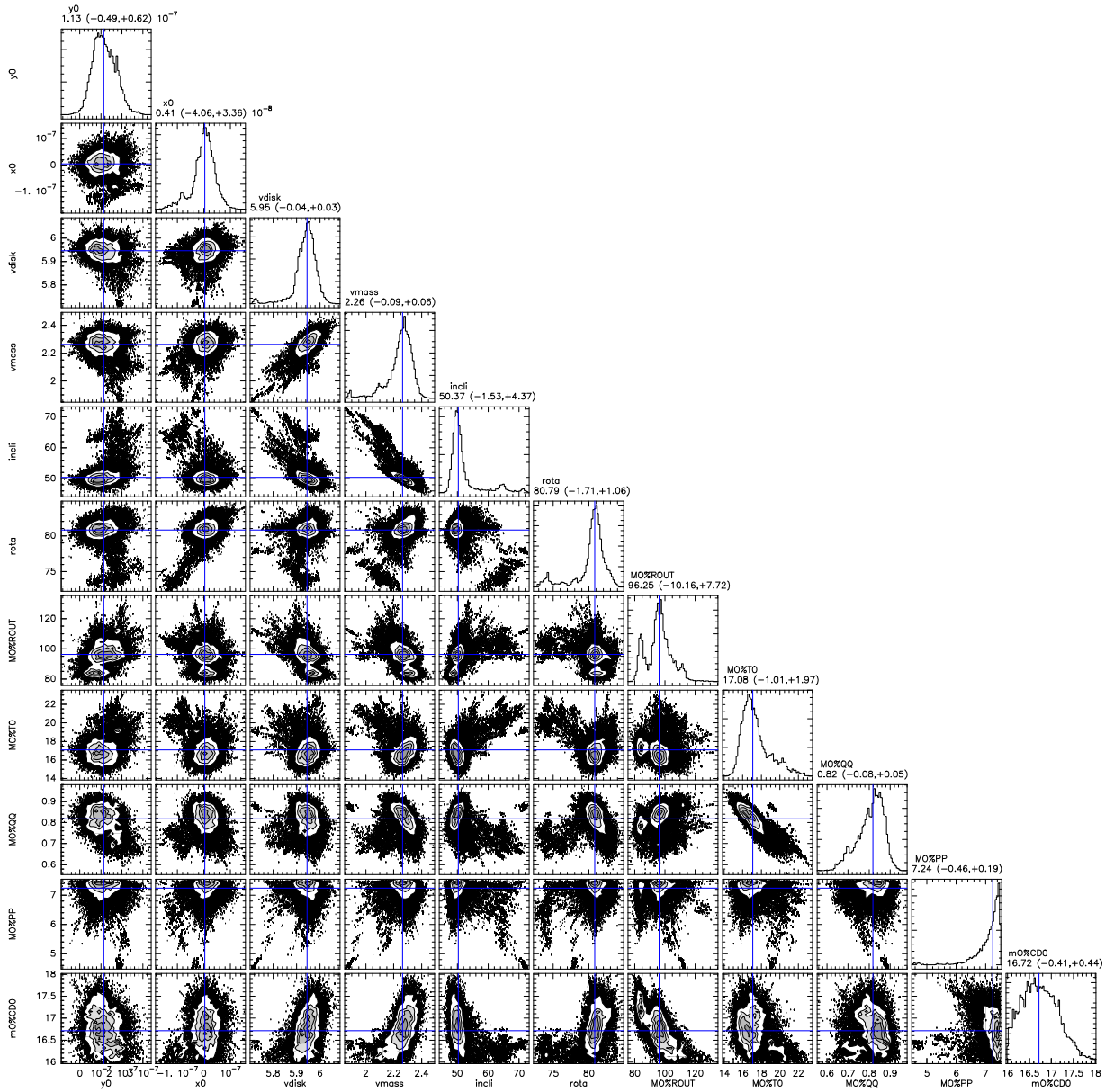


Figure B11. Correlation plot for parameters of the HK Tau A disk resulting from an MCMC analysis.